Spectroscopy investigation of nanostructured nickel-zinc ferrite obtained by mechanochemical synthesis

Z. Ž. LAZAREVIĆ[a,*], Č. JOVALEKIĆ[b], A. MILUTINOVIĆ[a], N. DANEU[c], M. ROMČEVIĆ[a], Đ. JOVANOVIĆ[a], N. ROMČEVIĆ[a]

*a*Institute of Physics, University of Belgrade, P.O. Box 68, Belgrade, Serbia
*b*The Institute for Multidisciplinary Research, University of Belgrade, Serbia
*c*Department for Nanostructured Materials, Jožef Stefan Institute, Ljubljana, Slovenia

Nickel-zinc ferrite, $Ni_{0.5}Zn_{0.5}Fe_2O_4$ was prepared by a soft mechanochemical route from mixtures of $Ni(OH)_2$, $Zn(OH)_2$ and $Fe(OH)_3$ powders in a planetary ball mill. The mechanochemical treatment provoked reaction leading to the formation of the $Ni_{0.5}Zn_{0.5}Fe_2O_4$ spinel phase what was monitored by XRD, TEM, SEM, IR and Raman spectroscopy. The spinel phase was first observed after 5h of milling and its formation was completed after 10 h. The synthesized $Ni_{0.5}Zn_{0.5}Fe_2O_4$ has a nanocrystalline structure with a crystallite size of about 16 nm. Four active modes are seen in the far-infrared reflectivity spectra. The Raman spectrum suggests an existence of mixed spinel structure in the obtained nano-powder samples.

1. Introduction

Spinel ferrites have attracted intense interest in fundamental science, especially for addressing the basic relationship between magnetic properties and their crystal chemistry and structure [1-3]. The spinel structure is shown in Fig. 1. Ferrites have been extensively investigated in recent years for their useful electrical and magnetic properties and applications in information storage systems, magnetic bulk cores, magnetic fluids, microwave absorbers and high frequency devices [4, 5]. Among the spinel ferrites, Ni-Zn ferrite is a magnetic material that is much used by the modern electronics industry due to its high electrical resistivity, high values of magnetic permeability, low dielectric loss, together with high mechanical strength, good chemical stability, and low coercivity [6].
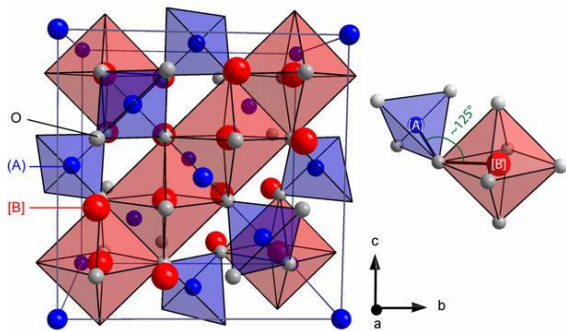

Fig. 1. The cubic unit cell of spinel oxides consists of 56 ions: 32 anions (O^{2-}) and 24 cations. In ternary spinel ferrites, MFe_2O_4, M and Fe cations are distributed over the sites of tetrahedral (A) and octahedral [B] coordination.

It is well known that nickel ferrite has an inverse spinel structure with Ni^{2+} ions at octahedral [B] sites and Fe^{3+} ions equally distributed at tetrahedral (A) and octahedral [B] sites. Whereas, zinc ferrite has a normal spinel structure with Zn^{2+} ions at A-sites and Fe^{3+} ions at B-sites. Therefore, when Ni^{2+} is substituted with Zn^{2+} in $Ni_{1-x}Zn_xFe_2O_4$, the cation distribution can be represented as $(Zn^{2+}_xFe^{3+}_{1-x})[Ni^{2+}_{1-x}Fe^{3+}_{1+x}]O^{2-}_4$ [7].

Since the particle size is reduced to a nanometer level, $NiFe_2O_4$ and $ZnFe_2O_4$ show a change of magnetic ordering [8, 9] and a magnetic moment that is attributed to the cation redistribution in the form of a mixed spinel structure with variation of 'x' depending on the thermal history [10]. Indeed, nanostructured materials exhibit unusual physical and chemical properties, significantly different from those of the bulk materials due to their extremely small size or large specific surface area [11]. The spinel ferrite powders are usually prepared through conventional solid-state reaction [12, 13], sol-gel technique [14, 15], hydrothermal synthesis [16], co-precipitation [8, 17] and mechanochemical process [18]. Mechanochemical synthesis is the general name given to the process of milling of powders which is accompanied by chemical reactions. It was first developed for the preparation of intermetallic compounds and nano-crystalline alloys. Novel approach to mechanochemical synthesis, based on reactions of solid acids, based hydrated compounds, crystal hydrates, basic and acidic salts, has been called soft mechanochemical synthesis [19]. The dissolved substances in the solid state substantially change their nature. It can influence on the comparison and properties of the final product. Peculiarities of soft mechanochemical reactions consist in the high reactivity of surface functional groups, notably, OH groups [19-21].

The major advantages of soft mechanochemical synthesis lie in the formation of reaction products at a room or a low temperature and the refinement of produced powders to a nanometer size range. This is reflected primarily in the simplicity of the procedure and equipment used. In many cases, when it comes to classical synthesis reaction sintering process, requires high temperatures, which can present an additional problem in industrial production. Mechanochemical derived precursors exhibit significantly higher reactivity and thus lower the sintering temperature.

Previously, we have used this method synthesis to prepare Mn-, Ni- and $ZnFe_2O_4$ ferrites [22]. The objective of present work is primarily to prepare the $Ni_{0.5}Zn_{0.5}Fe_2O_4$ ferrite by soft mechanochemical synthesis and to study this ferrite using different methods of characterization.

2. Experimental procedures

For mixtures of crystalline powders, the starting material were: nickel(II)-hydroxide ($Ni(OH)_2$, Merck 95% purity), zinc(II)-hydroxide ($Zn(OH)_2$, Merck 95% purity) and iron-hydroxide ($Fe(OH)_3$) in equimolar ratio. Soft mechanochemical synthesis was performed in air atmosphere in planetary ball mill (Fritsch Pulverisette 5) for 10 h. Characterization of the obtained samples was carried out by several methods.

The formation of phase of the $Ni_{0.5}Zn_{0.5}Fe_2O_4$ was verified via the X-ray diffraction measurements (XRD). Model Philips PW 1050 diffractometer equipped with a PW 1730 generator (40 kV x 20 mA) was used with Ni filtered CoKα radiation of 1.78897 Å at the room temperature. Measurements were done in 2θ range of 15-80° with scanning step width of 0.05° and 10 s scanning time per step.

Raman measurement of the obtained powder was performed using Jobin-Ivon spectrometer. An optical microscope with 100x objective was used to focus the 514 nm radiation from a Coherent Innova 99 Ar^+ laser on the sample. The backscattered light was collected by a charge-coupled device (CCD) detection system. Room temperature Raman spectra are in spectral range from 100 to 800 cm^{-1}.

The reflectivity measurements were carried out with a BOMMEM DA-8 spectrometer. A DTGS pyroelectric detector was used to cover the wave number range from 50-700 cm^{-1}.

TEM studies were performed using a 200 kV TEM (JEM-2100 UHR, Jeol Inc., Tokyo, Japan) equipped with an ultra-high resolution objective lens pole piece having a point-to-point resolution of 0.19 nm, being sufficient to resolve the lattice images of nanoparticles. Due to relatively small size of the nanoparticles selected area electron diffraction patterns (EDP) over the multiple nanocrystals was recorded to obtain the characteristic diffraction rings with structure-specific d-values.

The morphology of powder sample of soft Ni-Zn ferrite was synthesized by planetary mill and the size of crystallite was examined by Scanning Electron Microscopy SEM (JEOL JSM-5200).

3. Results and discussion

The X-ray diffraction pattern of ferrite sample having general formula $Ni_{(1-x)}Zn_{(x)}Fe_2O_4$ where x = 0.5 are shown in Fig. 2. The diffractogram of the mixtures of starting $Ni(OH)_2/Zn(OH)_2/Fe(OH)_3$ hydroxide powders, Fig. 2, suggests that hydroxides are amorphous (0 h of milling). After 10 h of milling, there are no traces of starting materials, ie any other intermediate reaction product. The pattern was indexed using PCPDFWIN data (PDF #52-0278) for Ni-Zn ferrite. There are no extra peaks indicating purity of the sample synthesized. The positions of the Bragg lines were used to obtain the interplanar spacing, Table 1. The result is in agreement with the reports in the literature [12]. The average crystallite size (L) obtained from the most intense line (3 1 1) was (16 nm) as estimated by Scherrer equation as follows [23]:

$$L = K \lambda_{Co} / (\beta \cos \theta_{hkl})$$

where L is the crystallite size, λ_{Co} is the wavelength of X-ray radiation (1.78897 Å for Co-K_α), θ_{hkl} is the Bragg angle and β is the full width at half maximum (FWHM) of the diffraction peak (reflection from (hkl) crystal plane) reduced for instrumental broadening. K is a Scherrer constant.

The obtained XRD patterns show clear peaks whose positions and relative intensities correspond to the bulk $Ni_{0.5}Zn_{0.5}Fe_2O_4$ and are well indexed as cubic spinel phase with the *fcc* structure [16]. The diffractograms show different reflection planes indexed as (hkl): (111), (220), (311), (222), (400), (422), (511) and (440). Based on the measured positions of diffraction peaks it can be calculated lattice constant by well-known relation for cubic crystals:

$$a = \lambda_{Co} (h^2 + k^2 + l^2)^{1/2}/(2\sin\theta_{hkl})$$

Calculated lattice constant for obtained nanopowder $Ni_{0.5}Zn_{0.5}Fe_2O_4$ is 8.3734 Å (in PCPDFWIN data is given a = 8.382 Å for bulk).
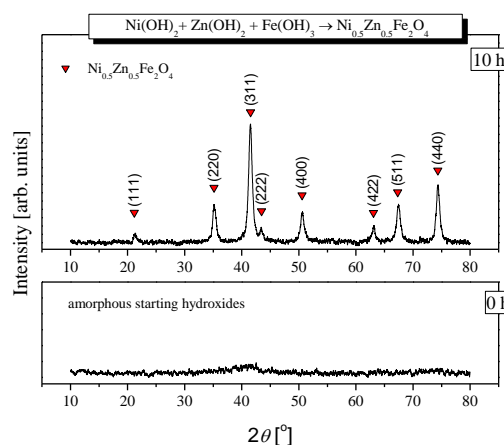

Fig. 2. X-ray diffraction patterns of the mixture of amorphous starting $Ni(OH)_2/Zn(OH)_2/Fe(OH)_3$ hydroxide powders and the $Ni_{0.5}Zn_{0.5}Fe_2O_4$ obtained for 10 h of milling time.

Table 1. Calculated d-values from XRD data and from EDP.

hkl	d_{XRD} (nm)	ring no.	d_{EDP} (nm)
(111)	0.4834	1	0.4841
(220)	0.2960	2	0.2959
(311)	0.2546	3	0.2531
(400)	0.2093	4	0.2093
(422)	0.1709	5	0.1707
(511)	0.1611	6	0.1619
(440)	0.1481	7	0.1482

Fig. 3. Raman spectra at room temperature of the Ni$_{0.5}$Zn$_{0.5}$Fe$_2$O$_4$ obtained for 10 h milling time.

The structure of normal spinel (like bulk ZnFe$_2$O$_4$) is face-centered space group Fd3m [O$_h^7$], with 8M^{II}Fe$_2^{III}$O$_4$ units per full unit cell containing 56 atoms, and the smallest Bravais cell consists of 2 formula units with 14 atoms [24]. The irreducible representation at the zone center modes could be described as follows by factor group analysis [25]:

$$\Gamma = A_{1g}(R) + E_g(R) + F_{1g} + 3F_{2g}(R) + 2A_{2u} + 2E_u + 4F_{1u}(IR) + 2F_{2u}$$

where *R* and *IR* denote Raman and infrared activity of the modes, respectively. There are predicted five symmetry-allowed, first-order Raman active modes ($A_{1g} + E_g + 3F_{2g}$) and four IR active modes. It is common to use this representation for inverse or partially inverse spinels for the sake of simplicity.

In the present study of Ni$_{0.5}$Zn$_{0.5}$Fe$_2$O$_4$ more than 5 Raman modes are visible in Fig. 3. Compared with Ref-s. [25-28], these peaks are characteristics for Ni-Zn ferrite. More than five peaks in Raman spectra are the consequence of the inversion of cations, as well as the existence of three types of cations. The analysis of the deconvoluted spectrum shows that above 600 cm^{-1} are 3 modes with A$_{1g}$ symmetry, originated from symmetric stretching of oxygen tetrahedrons with different cations inside. At the lowest wave number, about 636 cm^{-1}, is a contribution of the most massive Zn^{2+}-ions in tetrahedral surrounding, followed by Ni^{2+} at about 687 cm^{-1} and Fe^{3+} at 720 cm^{-1}. Similar situation is with other Raman modes, also. E$_g$ modes (two of them are separated) are due to symmetric bending of oxygen with respect to cations in tetrahedral surrounding. F$_{2g}$(2) and F$_{2g}$(3) correspond to the vibrations of octahedral group. F$_{2g}$(1) are due to translational movement of the whole tetrahedrons.

Small intensity of Fe-O$_4$ component of A$_{1g}$ mode and high intensity of Ni-O$_4$ component suggest that there is a small amount of Fe^{3+} ions, but high amount of Ni^{2+} in tetrahedral sites, what implies that cations are redistributed.
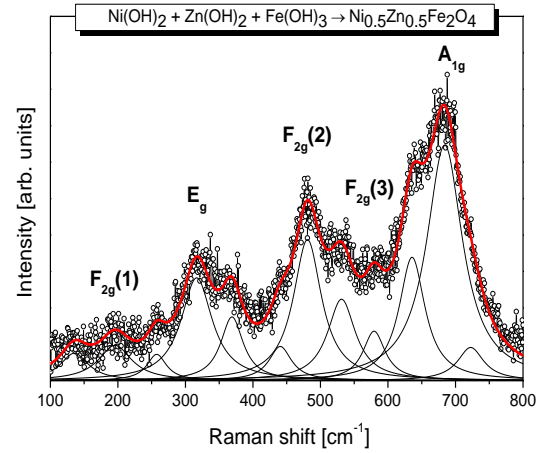
Far infrared reflectivity spectra of the synthesized Ni$_{0.5}$Zn$_{0.5}$Fe$_2$O$_4$ ferrite were recorded at room temperature, Fig. 4. Expectedly weak intensity of the reflectivity spectrum of nanopowder and broadness of the recorded IR modes don't allow separation of the different cations contributions in the observed bands. The highest energy band F$_{1u}$(4) at ~ 580 cm^{-1} corresponds to the vibrations of cation-oxygen bonds in tetrahedral sites and the lower band F$_{1u}$(3) at ~ 360 cm^{-1} is attributed to the vibrations of the cation-oxygen bond in octahedral site.

FIR spectrum, presented at Fig. 4 is fitted by plasmon - phonon interaction model of dielectric function [29, 30]:

$$\varepsilon = \varepsilon_\infty \left(\prod_i^n \frac{\omega_{LO_i}^2 - \omega^2 - j\omega\gamma_{LO_i}}{\omega_{TO_i}^2 - \omega^2 - j\omega\gamma_{TO_i}} - \frac{\omega_p^2}{\omega^2 + j\omega\gamma_p} \right),$$

where $\omega_p = \sqrt{\dfrac{ne^2}{4\pi\varepsilon_0\varepsilon_\infty m^*}}$ [rad s^{-1}].

The first term in equation is the lattice vibration contribution, whereas the second term is the Drude term for the free-carrier contribution to the dielectric constant. $\omega_{LO(TO)}$ are longitudinal (transverse) frequencies and $\gamma_{LO(TO)}$ their dampings, ω_p is plasma frequency, γ_p plasma damping, *n* free charier concentration, m^* their effective mass, ε_0 is dielectric constant of vacuum (8.854·10^{-12} F m^{-1}) *and* ε_∞ is the high frequency dielectric constant. Spectrum is fitted with one plasmon and 5 phonons. Besides 4 zone centre modes, it was necessary to introduce one mode more to describe a discrete feature in the low energy of FIR spectrum (probably activated by disorder). Fitting parameters are listed in Fig. 4. On the basis of obtained value of the plasma frequency, it is possible, knowing the effective mass, to estimate the concentration of free carriers, as $n = (4\pi\omega_p^2\varepsilon_0\varepsilon_\infty m^*)/e^2$. To our knowledge, the effective mass for various types of charge carriers is estimated only for SiMg$_2$O$_4$, SiZn$_2$O$_4$ and SiCd$_2$O$_4$ in Ref. [31]. An approximate value from the

mentioned study $m^* = 0.4 \cdot m_0$ was used in the calculation of carrier concentration and obtain $n = 5.4 \cdot 10^{18}$ cm^{-3}.

The concentration calculated from FIR measurement correspond to free band carriers that could be excited at a given temperature. Due to relatively wide energy gap in $Ni_xZn_{1-x}Fe_2O_4$ (1.9 - 2.26 eV) [32, 33], amount of these carriers is relatively small at ambient temperature.

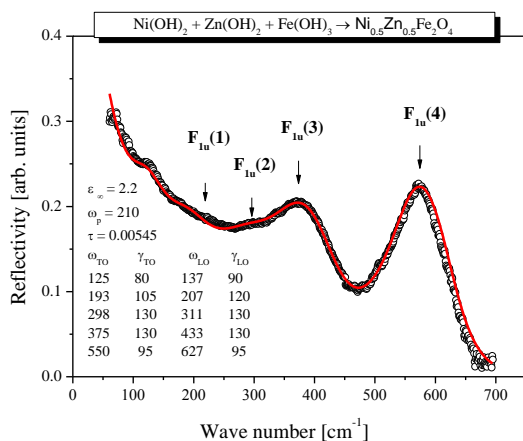*Fig. 4. IR spectrum of the Ni$_{0.5}$Zn$_{0.5}$Fe$_2$O$_4$ recorded at room temperature is presented by open circles; The fit of spectrum is presented by red line. Fitting parameters are given in the inset.*

The mechanochemical synthesis of $Ni_{0.5}Zn_{0.5}Fe_2O_4$ is feasible and complete after 10 h milling time. This is considerably less time compared with the time (346.5 ks or 96 h) for which the spinel $Ni_{0.5}Zn_{0.5}Fe_2O_4$ obtained in the work by Todaka and co-authors [34]. It can be seen that the nanoparticles are about 30 nm in diameter. Fig. 5 shows the TEM micrograph for the sample obtained from the mixture of $Ni(OH)_2$, $Zn(OH)_2$ and $Fe(OH)_3$ powders by the soft mechanochemical synthesis for 10 h milling time. TEM analysis on our sample revealed that ferrite sample is composed of nanosized particles with size around 20 nm, what is in accordance with obtained XRD-value (16 nm). Jovalekić and co-authors [18] were synthesized nanocrystalline $Ni_{0.5}Zn_{0.5}Fe_2O_4$ in a high energy planetary mill starting from the NiO, ZnO and Fe_2O_3 oxide powders. The obtained nickel-zinc ferrite has many inhomogeneities and a distorted spinel structure.
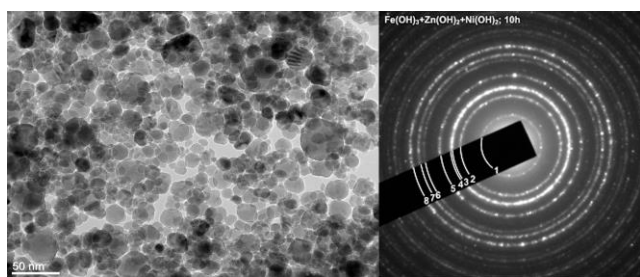

Fig. 5. TEM micrograph image and electron diffraction patterns (Debye-Sherrer rings) of the Ni$_{0.5}$Zn$_{0.5}$Fe$_2$O$_4$ ferrite sample obtained by milling for 10h from the mixture of Ni(OH)$_2$, Zn(OH)$_2$ and Fe(OH)$_3$ hydroxide powders.

TEM analysis revealed that ferrite sample is composed of roundish nanosized particles with size around 20 nm, what is in accordance with obtained XRD-value (16 nm). In the Fig. 5 electron diffraction pattern (EDP) is given. The calculated d-values for one sample are shown in Table 1 together with values obtained from XRD-analysis.

SEM micrograph (Fig. 6) shows powder sample of $Ni_{0.5}Zn_{0.5}Fe_2O_4$ ferrite that was synthesized by planetary mill synthesis procedure. The nanoscale crystallite tend to agglomerate because of the dipolar feild of each crystallite [35]. Agglomerated crystallites form grains with sizes substantially greater than 20 nm.
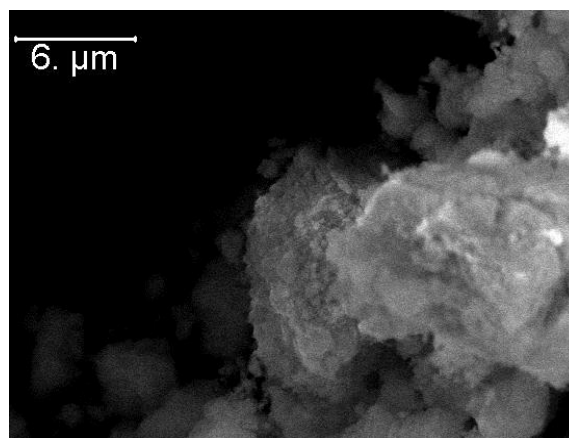

Fig. 6. SEM image of the Ni$_{0.5}$Zn$_{0.5}$Fe$_2$O$_4$ ferrite sample obtained by milling for 10h from the mixture of Ni(OH)$_2$, Zn(OH)$_2$ and Fe(OH)$_3$ hydroxide powders.

4. Conclusions

In this paper, we obtained $Ni_{0.5}Zn_{0.5}Fe_2O_4$ ferrite by soft mechanochemical synthesis starting from the mixture of appropriate amounts of hydroxide powders. It has been shown that mechanochemical treatment of mixture with starting materials leads to forming the pure phase of $Ni_{0.5}Zn_{0.5}Fe_2O_4$ after 10 h of milling. In the Raman and IR spectra are observed all of the group theory predicted first-order active modes characteristic for spinel structure.

References

[1] M. A. Gabal, Reda M. El-Shishtawy, Y. M. Al Angari, J. Magn. Magn. Mater. **324**, 2258 (2012).
[2] D. S. Mathew, R. S. Juang, Chem. Eng. J. **129**, 51

(2007).

[3] K. M. Batoo, Nanoscale Res. Lett. **6**, 499 (2011).

[4] M. Atif, M. Nadeem, R. Grössinger, R. Sato Turtelli, J. Alloy Compd. **509**, 5720 (2011).

[5] J. L. Dorman, D. Fiorani (Eds.), Magnetic Properties of Fine Particles, Amesterdam, North-Holland, 1992.

[6] E. S. Murdock, R. F. Simmons, R. Davidson, IEEE Trans. Magn. **28**, 3078 (1992).

[7] J. Smit, H. P. J. Wijn, Ferrites-Physical Properties of Ferrimagnetic Oxides in Relation to Their Technical Applications, N. V. Philip's Gloeilampenfabrieken, Eindhoven/Holland, 1959 (Chap. VIII), pp. 136-176.

[8] D. G. Chen, X. G. Tang, J. B. Wu, W. Zhang, Q. X. Liu, Y. P. Jiang, J. Magn. Magn. Mater. **323**, 1717 (2011).

[9] G. F. Goya, H. R. Rechenberg, J. Magn. Magn. Mater. **203**, 141 (1999).

[10] M. Ajmal, A. Maqsood, Mater. Sci. Eng. B **139**, 164 (2007).

[11] H. Yang, X. C. Zhang, W. Q. Ao, G. Z. Qiu, Mater. Res. Bull. **39**, 833 (2004).

[12] Abdul Samee Fawzi, A. D. Sheikh, V. L. Mathe, J. Alloy Compd. **502**, 231 (2010).

[13] Dong-Lin Zhao, Qiang Lv, Zeng-Min Shen, J. Alloy Compd. **480**, 634 (2009).

[14] Hong-Wen Wang, Shong-Chung Kung, J. Magn. Magn. Mater. **270**, 230 (2004).

[15] Jeevan Job Thomas, A. B. Shinde, P. S. R. Krishna, Nandakumar Kalarikkal, J. Alloy Compd. **546**, 77 (2013).

[16] R. M. Freire, T. S. Ribeiro, I. F. Vasconcelos, J. C. Denardin, E. B. Barros, Giuseppe Mele, L. Carbone, S. E. Mazzetto, P. B. A. Fechine, J. Nanopart. Res. **15**, 1616 (2013).

[17] T. J. Shinde, A. B. Gadkari, P. N. Vasambekar, J. Magn. Magn. Mater. **333**, 152 (2013).

[18] Č. Jovalekić, A. S. Nikolić, M. Gruden-Pavlović, M. Pavlović, J. Serb. Chem. Soc. **77**, 497 (2012).

[19] E. Avvakumov, M. Senna, N. Kosova, Soft Mechanochemical Synthesis: A Basis For New Chemical Technologies, Kluwer Academic Publishers, Boston, 2001.

[20] M. Senna, Solid State Ionics **63-65**, 3 (1993).

[21] V. V. Boldyrev, Solid State Ionics **63-65**, 537 (1993).

[22] Z. Ž. Lazarević, Č. Jovalekić, A. Milutinović, D. Sekulić, M. Romčević, M. Slankamenac, N. Ž. Romčević, Optoelectron. Adv. Mater. **7**, 720 (2013).

[23] Scherrer and Warren equations (B. E. Warren, X-ray Diffraction, Addison Wesley: Reading MA, (1969).

[24] W. B. White, B. A. Deangelis, Spectrochim. Acta A **23**, 985 (1957).

[25] Z. W. Wang, D. Schiferl, Y. S. Zhao, H. St. C. O'Neilr, J. Phys. Chem. Solids **64**, 2517 (2003).

[26] T. Yu, Z. X. Shen, Y. Shi, J. Ding, J. Phys. Condens. Matter. **14**, L613 (2002).

[27] Z. H. Zhou, J. M. Xue, J. Wang, H. S. O. Chan, T. Yu, Z. X. Shen, J. Appl. Phys. **91**, 6015 (2002).

[28] Z. H. Zhou, J. M. Xue, H. S. O. Chan, J. Wang, Mater. Chem. Phys. **75**, 181 (2002).

[29] A. Barker, Phys. Rev. **136,** A1290 (1964).

[30] D. Berreman, F. Unterwald, Phys. Rev. **174**, 791 (1968).

[31] D. Allali, A. Bouhemadou, E. Muhammad Abud Al Safi, S. Bin-Omran, M. Chegaar, R. Khenata, A. H. Reshak, Physica B **443**, 24 (2014).

[32] P. H. Borse, J. S. Jang, S. J. Hong. J. S. Lee, J. H. Jung, T. E. Hong, C. W. Ahn, E. D. Jeong, K. S. Hong, J. H. Yoo, H. G. Kim, J. Korean Phys. Soc. **55**, 1472 (2009).

[33] M. Meinert, G. Reiss, J. Phys. Condens. Matter. **26**, 115503 (2014).

[34] Y. Todaka, M. Nakamura, S. Hattori, K. Tsuchiya, M. Umemoto, Mater. Tran. **44**, 277 (2003).

[35] E. Manova, B. Kunev, D. Paneva, I. Mitov, L. Petrov, C. Estournes, C. D. Orleans, J.-L. Rehspringer, M. Kurmoo, Chem. Mater. **16**, 5689 (2004).

_____
[*]Corresponding author: lzorica@yahoo.com